Earth Surf. Dynam. Discuss., doi:10.5194/esurf-2016-64, 2017
Manuscript under review for journal Earth Surf. Dynam.
Published: 10 January 2017

Earth Surface Dynamics Discussions
Open Access
EGU

Single-block rockfall dynamics inferred from seismic signal analysis

Clément Hibert[1], Jean-Philippe Malet[1], Franck Bourrier[2], Floriane Provost[1], Frédéric Berger[2], Pierrick Bornemann[1], Pascal Tardif[2], and Eric Mermin[2]

[1]Institut de Physique du Globe de Strasbourg - CNRS UMR 7516, University of Strasbourg/EOST, France
[2]Institut national de recherche en sciences et technologies pour l'environnement et l'agriculture (IRSTEA), 2 Rue de la Papeterie, 38402 Saint-Martin-d'Hères, France

Correspondence to: Clément Hibert (hibert@unistra.fr)

Abstract. We conducted controlled releases of single blocks within a soft-rock (black marls) gully of the Rioux Bourdoux torrent (French Alps). 28 blocks, with masses ranging from 76 kg to 472 kg, were used for the experiment. An instrumentation combining video cameras and seismometers was deployed along the traveled path. The video cameras allow to reconstruct the trajectories of the blocks and to estimate their velocities at the time of the different impacts with the slope. These data are compared to the recorded seismic signals. As the distance between the falling block and the seismic sensors at the time of each impact is known, we were able to determine the associated seismic signal amplitude corrected from propagation and attenuation effects. We compared the velocity, the loss of potential energy, the kinetic energy and the momentum of the block at each impact to the true amplitude and the energy of the corresponding part of the seismic signal. Our results suggest that the amplitude of the seismic signal scales with the momentum of the block at the impact. We also found a scaling law between the potential energy lost, the kinetic energy and the energy of the seismic radiation generated by the impacts. By combining these scaling laws, we inferred the mass and the velocity before impact of each block directly from the seismic signal. Despite high uncertainties, the values found are close to the true values of the mass and the velocities of the blocks. These relationships also provide new insights to understand the source of high-frequency seismic signals generated by rockfalls.

1 Introduction

Understanding the dynamics of rockfalls and other mass movements is critical to mitigate the associated hazards but is very difficult because of the limited number of observations of natural events. With the increasing densification of the global, regional and local seismometer networks, seismic detection of gravitational movements is now possible. The continuous recording ability of seismic networks allows a reconstruction of the gravitational activity at unprecedented time scale. More than the detection of these events, recent advances allow to determine the dynamics of the largest landslides on Earth from the very low-frequency seismic waves they generate. Inversion and modeling of the long-period seismic waves permits to infer the force imparted by these catastrophic events on Earth, and to deduce dynamic parameters (acceleration, velocity, trajectory) as well as their mass (Favreau et al., 2010; Schneider et al., 2010; Moretti et al., 2012; Ekström and Stark, 2013; Allstadt, 2013; Yamada et al., 2013; Hibert et al., 2014a, c). However, these approaches are limited by the size of the events. Only the largest landslides

Earth Surf. Dynam. Discuss., doi:10.5194/esurf-2016-64, 2017
Manuscript under review for journal Earth Surf. Dynam.
Published: 10 January 2017

will generate the long-period seismic waves used in the inversion and the modeling methods. These events constitute only a small proportion of the landslides that occur worldwide.

In recent years, a new approach based on the analysis of the high-frequency seismic signal has been proposed. High-frequency seismic waves are generated independently of the size of the event, and can be recorded, if seismometers are close enough to the source. Hence, this allows a seismic detection of the events that do not generate long-period seismic waves (e.g. Deparis et al., 2008; Helmstetter and Garambois, 2010; Dammeier et al., 2011, 2016; Hibert et al., 2011, 2014b; Clouard et al., 2013; Chen et al., 2013; Burtin et al., 2013; Tripolitsiotis et al., 2015; Zimmer and Sitar, 2015). The limitation of this approach is that high-frequency seismic waves are more prone to be influenced by propagation effects (attenuation, dispersion, scattering) and, more importantly, that the source of the high-frequency seismic waves associated with gravitational instabilities is not well understood yet.

Several studies have shown that some landslide properties can be linked to features of the high-frequency seismic signals. In some cases, it has been shown that the landslide volumes can be linked to the amplitude (Norris, 1994; Dammeier et al., 2011) or to the energy of the high-frequency seismic signals (Hibert et al., 2011; Yamada et al., 2012). Several studies have shown that the high-frequency seismic signals can also carry information on the landslide dynamics. Schneider et al. (2010) have shown, thanks to numerical modeling, that a good correlation exists between the short-period seismic-signal envelope, the modeled friction work rate and the momentum (product of the mass and the velocity) for two rock-ice avalanches. The model-based approach proposed by Levy et al. (2015) has shown that a correlation can be found between the modeled force and the power of the short-period seismic signal for rockfalls that occurred at the Soufrière Hills volcano on Montserrat Island. Hibert et al. (2017) have shown that, for 11 large landslides that occurred worldwide, the bulk momentum controls at the first order the amplitude of the envelope of the generated seismic signal. The authors also demonstrated that the maximum amplitude of the seismic signal, corrected from propagation effects, scales with the bulk momentum. These results are important as they open the perspective to quantify the landslide dynamics, independently of their size, and directly from the seismic signals they generate (i.e. without inversion or modeling). Being capable of quantifying the landslide properties directly from their seismic signals is critical for the development of future methods for their detection and characterization using high-frequency seismic signal in real-time. However, before considering an operational implementation of such methods, we need to better understand the source of the high-frequency seismic radiations associated, and the observations made on the link between these radiations and the landslide dynamics.

One of the assumptions that emerges from these studies to explain the link between the landslide dynamics and the high-frequency seismic signal features is that this relationship can potentially reflects the scaling of small-scale processes within the landslide mass, and between the landslide mass and the substrate. The impulse imparted to the solid Earth by a bouncing particle within a granular flow will be proportional to the kinematics of the particle, and the amplitude of the seismic wave will be proportional to the magnitude of the impulse. However, this assumption raises an important issue: what is the link between the dynamics of a single bouncing particle (a rock for example) and the seismic signal it generates?

Theoretical developments, laboratory and field experiments were conducted by Farin et al. (2015) to address this issue. The authors have shown that the mass and the speed of an impactor can be related to the radiated elastic energy at a given frequency,

Earth Surf. Dynam. Discuss., doi:10.5194/esurf-2016-64, 2017
Manuscript under review for journal Earth Surf. Dynam.
Published: 10 January 2017

Earth Surface Dynamics Discussions Open Access EGU

following analytic developments based on the Hertz theory of impact (Hertz, 1882). However, the field experiment conducted showed that, in this case, these simple relations did not perform well to quantify the velocity and the mass of single rocks from the seismic signal it generates. The major limitation they identified is that a great part of the energy liberated at the impact is lost in high frequencies (> 50 Hz), but the seismometer used during the field experiment was not capable of recording such high frequencies.

In this study we propose a new field experiment of controlled releases of single blocks to investigate the relations between block properties and dynamics, and the associated seismic signal features. We deployed several short-period and broadband seismic stations to record the seismic signal generated at each impact on soft-rock substrate. The trajectory of each block is reconstructed with video cameras. The seismic signal processing allowed us to retrieve the amplitude of the seismic signal at the source, corrected from propagation effects, and the energy of the seismic radiation generated by the impacts. We then compare the features of the seismic signal of each impact to the dynamics and the properties of the released block.

2 The Rioux Bourdoux experiment

The Rioux Bourdoux controlled releases experiment main focus is to study the seismic signal of single-block rockfalls on unconsolidated soft-rock, which are highly attenuating for seismic waves. The Rioux Bourdoux is a torrent located in the french Alps, approximately 4 km north of the town of Barcelonnette (France). The slopes surrounding the torrent consist mainly of Callovo-Oxfordian black-marls and are representative of the slopes morphology of marly facies observed in south-east France. Due to the high erosion susceptibility of black marls, and marls in general, numerous steep gullies have formed on these slopes.

We conducted our releases experiment within one of these gullies (Figure 1a and b). The advantage of launching the block in a gully is that for every block the traveled path is roughly similar. Moreover, the steepness of the gullies that developed in black-marls allows the block to rapidly reach a high velocity. The travel path had a length of approximately 200 meters and slope angles ranging from ~ 45 degrees on the upper part of the slope to ~ 20 degrees on the terminal debris cone. 28 blocks with mass ranging from 76 to 472 kg were manually launched.

Two video camera were deployed (Sony alpha7 - 25 frame per seconds) allowing to record the movement of the blocks. They were deployed at the feet of the gully, close to the torrent. Ground controlled points were marked for visual recognition on the videos and their 3D coordinates taken via GNSS. A reference Digital Elevation Model (DEM) at a spatial resolution of 0.5 m was built from terrestrial LIDAR acquisitions (Figure 1c). The time of the cameras was set to be synchronous with the seismic sensor time (GPS). The seismic monitoring device was composed of 1 broadband seismometer (CMG40T - sampling frequency 100 Hz) located north of the gully, and an antenna of 4 short-period seismometers (one 3 component and three with 1 vertical component - sampling frequency 1000 Hz) located south of the gully (Figure 1c).

Earth Surf. Dynam. Discuss., doi:10.5194/esurf-2016-64, 2017
Manuscript under review for journal Earth Surf. Dynam.
Published: 10 January 2017

Earth Surface Dynamics Discussions
Open Access
EGU

3 Methods

3.1 Trajectory reconstruction

To reconstruct the trajectory, the impacts of each block were manually picked on the frames of the videos. Thanks to the control points, the frames of the videos can be projected on the DEM. Hence, once an impact is identified on the frame, the position of the pixel is reported on the DEM, which gives the true position of the impact in space. This processing is repeated for the two cameras, which gives an estimate of the uncertainties on the position and the time of the impact. The velocity just before impact is derived from the block trajectory and the duration of block flight before impact. We also determined the potential energy lost during the block flight before impact from the difference of altitude of the block between two impacts, inferred from the reconstructed trajectory. Unfortunately, the resolution of the cameras and the complex dynamics of the blocks during the first seconds of propagation did not allow us to identify clearly the impacts on the upper part of the slope. However the trajectory of the blocks on the lower part of the slope is well constrained, with an average uncertainty on the inferred velocity of the blocks before impacts of 0.95 $\mathrm{m\,s^{-1}}$.

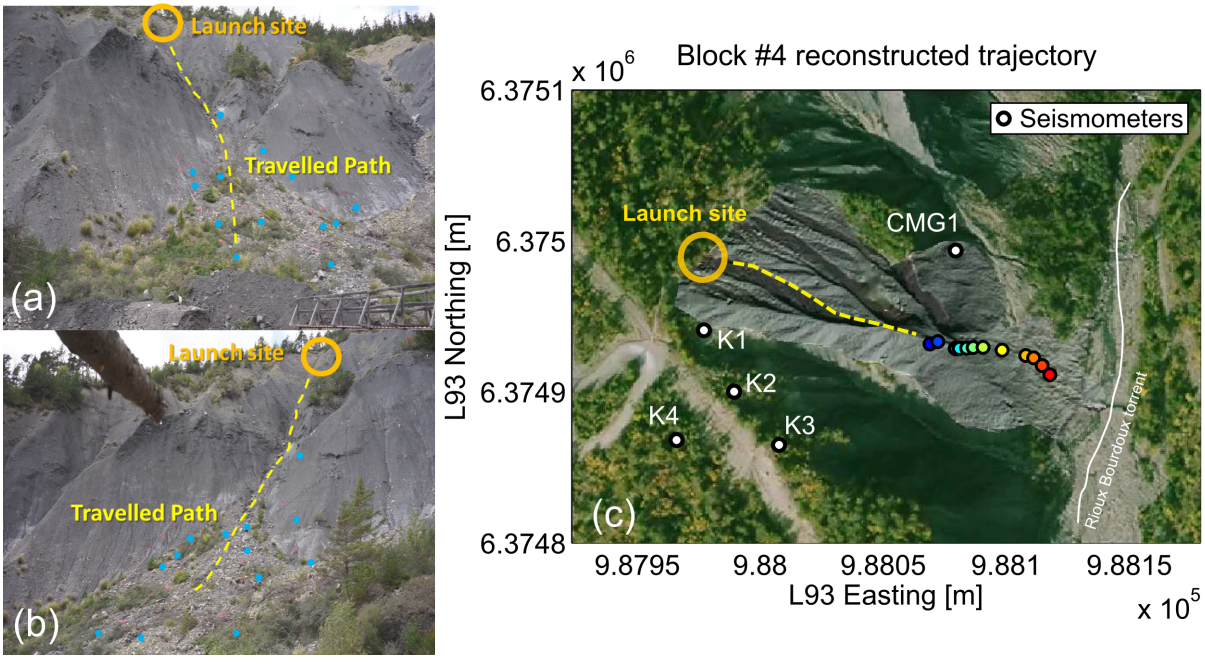

Figure 1. View from a) the first and b) the second video cameras deployed at the bottom of the slope. The ground control points are indicated by blue points. c) Trajectory reconstruction for block 4 on the DEM, built from LIDAR acquisition, superimposed on an orthophoto of the Rioux Bourdoux slopes.

Earth Surf. Dynam. Discuss., doi:10.5194/esurf-2016-64, 2017
Manuscript under review for journal Earth Surf. Dynam.
Published: 10 January 2017

3.2 Seismic signal processing

Seismic waves are subjected to strong propagation effects, especially in a highly attenuating medium such as black marls. Figure 2 shows the seismic signals recorded for the launch of the block number 4. The attenuation is visible when comparing peaks in the seismic signal recorded at the station located on the upper part of the slope (Figure 2a) to the ones recorded at the station on the lower part of the slope (Figure 2c), for the same time. The amplitude of the peaks is clearly dependent of the distance between the impact and the seismic station. Moreover, Figure 2b shows the attenuation of the highest frequency with the distance of the source to the seismic station. To compare seismic signal features to the dynamic parameter of the rockfall, we have to correct these attenuation effects. Aki and Chouet (1975) proposed a simple attenuation law giving the amplitude $A(r)$ of a seismic surface wave recorded at a distance r as:

$$A(r) = \frac{1}{\sqrt{r}} A0 \times e^{-Br}. \tag{1}$$

If the distance between the station and the source is known, the computation of the amplitude at the source $A0$ is straightforward. However we have to determine the parameter B that accounts for the anelastic attenuation of seismic waves. If we consider r_i the distance between the source and station i and r_j the distance to station j we have:

$$B_{ij} = \frac{log(A(r_i)\sqrt{r_i}) - log(A(r_j)\sqrt{r_j})}{\sqrt{r_j} - \sqrt{r_i}}. \tag{2}$$

By combining Eq. (1) and Eq. (2), we can compute the amplitude at the source $A0$ for each pair of stations. This value is then averaged over all the pairs of stations, and the standard deviation gives an estimate of the uncertainty.

The other quantity that we want to compare to the dynamics of the block is the seismic energy. The seismic energy of a seismic surface wave can be computed as (Crampin, 1965):

$$E_s = \int_{t_i}^{t_f} 2\pi r \rho h c u_{env}(t)^2 e^{Br} dt, \tag{3}$$

with :

$$u_{env}(t) = \sqrt{u(t)^2 + Ht(u(t))^2}, \tag{4}$$

where Ht is the Hilbert transform of the seismic signal $u(t)$ used to compute the envelope $u_{env}(t)$, t_i and t_f the times of the beginning and the end of the seismic signal respectively, h the thickness and ρ the density of the layer through which the generated surface waves propagate, and c their phase velocity. The average velocity of surface waves in black-marls is approximately 300 m/s (Hibert et al., 2012; Gance et al., 2012), which, for seismic signal with central frequencies around

Earth Surf. Dynam. Discuss., doi:10.5194/esurf-2016-64, 2017
Manuscript under review for journal Earth Surf. Dynam.
Published: 10 January 2017

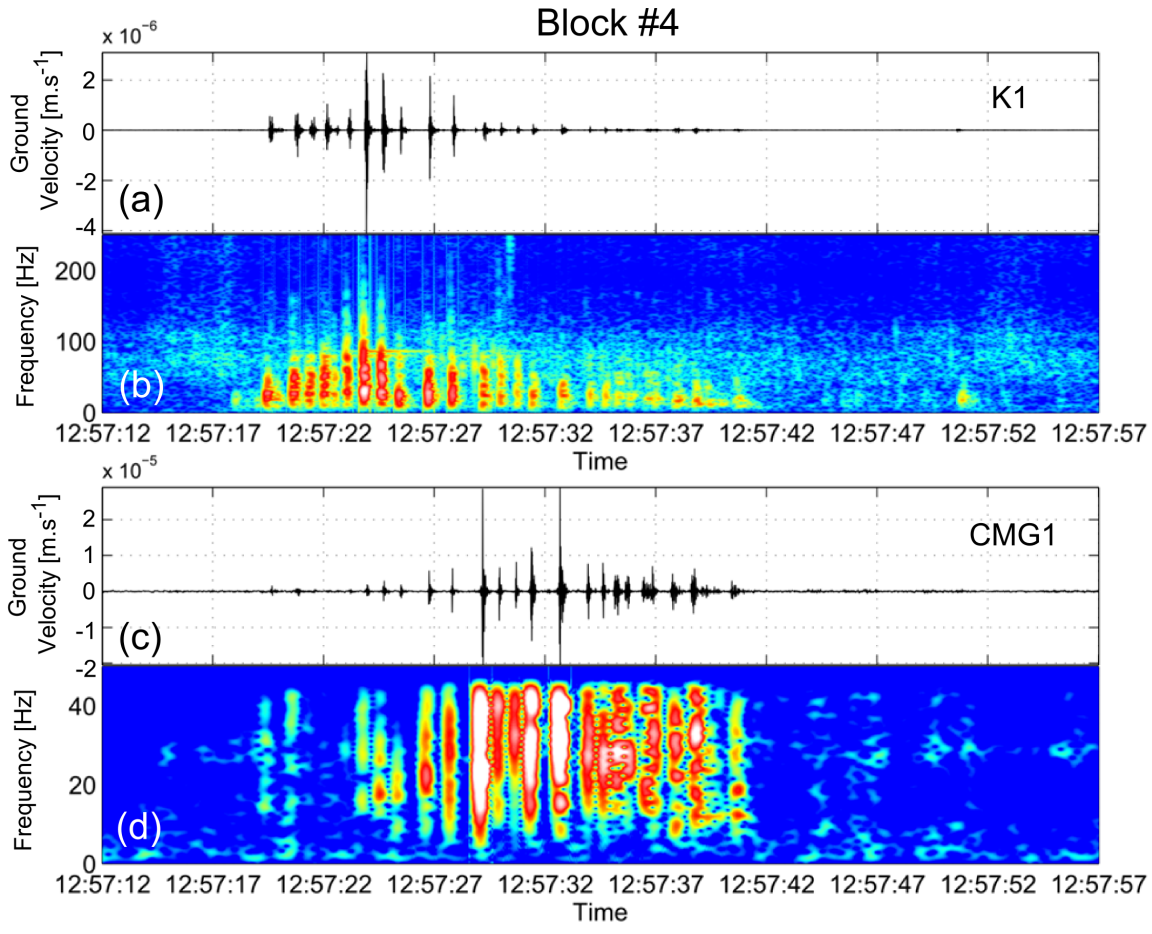

Figure 2. a) Signal recorded at the short-period station located on the upper part of the slope and b) corresponding spectrogram, generated by block number 4 (mass of 209 kg). c) Signal recorded at the broadband station located on the lower part of the slope and d) corresponding spectrogram, generated by block 4.

20 Hz (Figure 2), gives a propagation depth h of ~ 15 m. The density ρ of dry black-marls is approximately 1450 $\mathrm{kg\,m^{-3}}$ (Maquaire et al., 2003).

Before computing the amplitude at the source and the energy of the seismic signals generated by impacts, we first selected the seismic signals with the following criteria: i) we excluded from our analysis the seismic signals generated when sliding of the blocks occurred; ii) when the blocks stopped mid-slope and iii) more generally when the signal-to-noise ratio was too weak on the seismic stations to perform the computation of the parameter B. B is dependent on the frequency of the seismic waves. Therefore the seismic signals were band-pass filtered between 1 and 50 Hz. This frequency band is chosen because most of the seismic wave energy is not attenuated in this band within the span of the seismic network (Figure 2b and d). For each seismic

Earth Surf. Dynam. Discuss., doi:10.5194/esurf-2016-64, 2017
Manuscript under review for journal Earth Surf. Dynam.
Published: 10 January 2017

record selected, we manually picked the peaks corresponding to the impacts on each station. This processing results in a data set of 37 impact seismic signals, coming from 9 out of the 28 launches.

4 Results

4.1 Correlation between dynamic parameters and seismic signal features

From the reconstructed trajectories we inferred the velocity, the momentum and the kinetic energy of the block before each impact, and the potential energy lost during the block trajectory before impact. The velocities exhibit a low variability, with values ranging from 6 $\mathrm{m\,s^{-1}}$ to 17 $\mathrm{m\,s^{-1}}$ (Figure 3). We did not find significant correlation between the mass and the impact velocity.

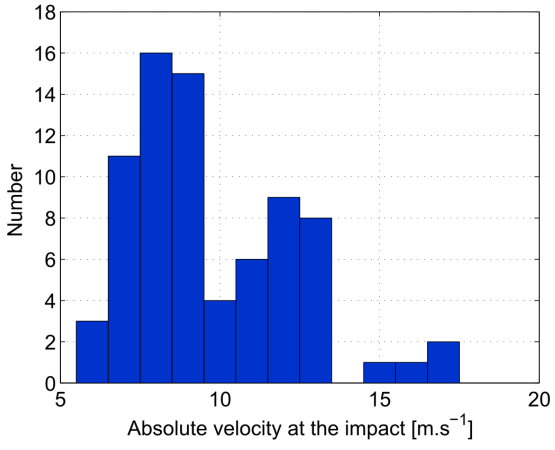

Figure 3. Histogram of the observed absolute velocities before impact.

The seismic signal processing allowed us to infer the amplitude at the source and the seismic energy of the seismic signal of the impacts. The average uncertainty on the computation of the maximum amplitude $A0_{max}$, inferred from the standard deviation, and expressed as a percentage of the computed values (i.e. $A0_{max} \pm x\% A0_{max}$), ranges from 7% to 129%, and is 58% in average. Regarding the computation of the seismic energy, the uncertainty, estimated following the same approach, ranges from 55% to 152% of the computed values, and is 86% in average.

We investigated the possible correlation between: 1) the maximum amplitude at the source $A0_{max}$ of the seismic signal and the absolute momentum $|p|$ before the impact; 2) the seismic energy E_s and the potential energy lost E_p; 3) the seismic energy and the kinetic energy E_k before impact; and 4) the seismic energy E_s and the mass m of the blocks. We computed for the

Earth Surf. Dynam. Discuss., doi:10.5194/esurf-2016-64, 2017
Manuscript under review for journal Earth Surf. Dynam.
Published: 10 January 2017

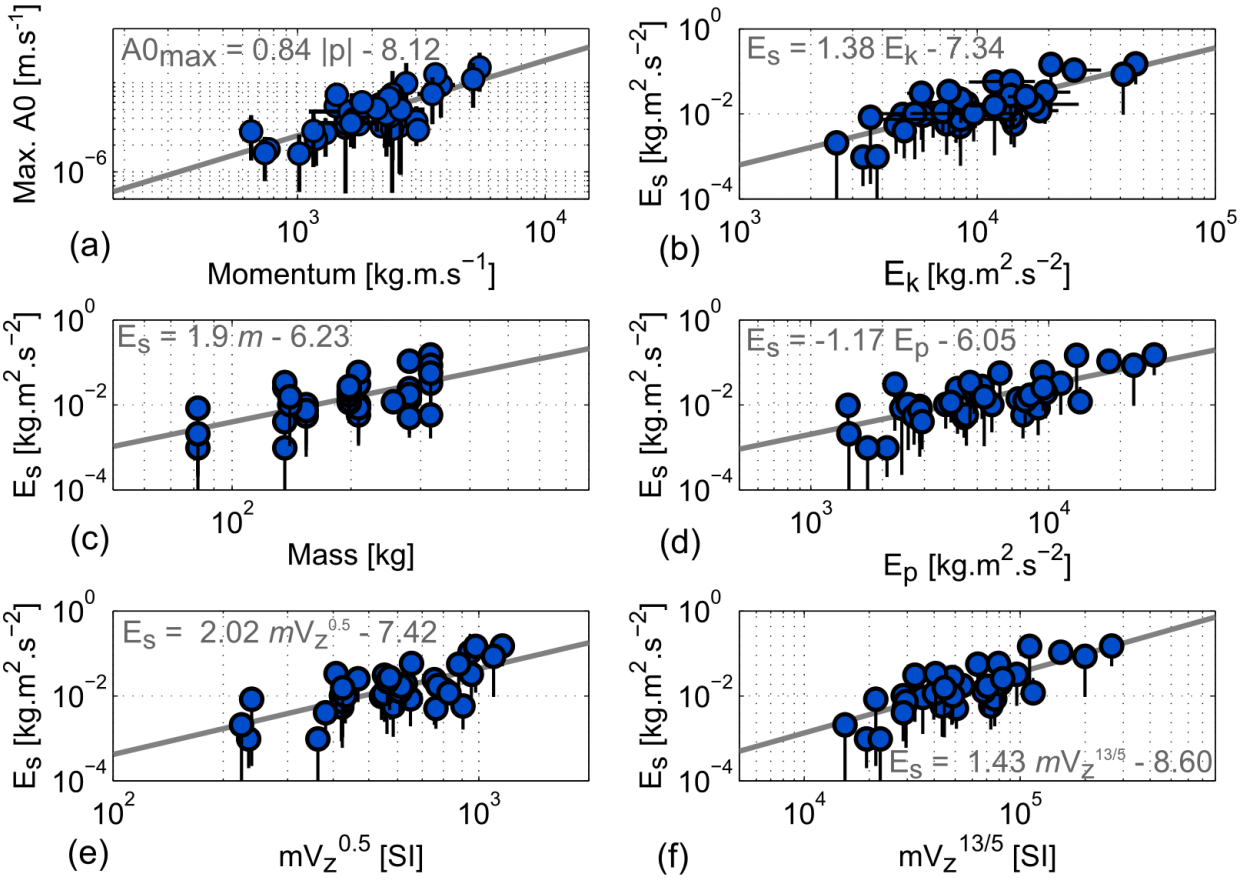

Figure 4. a) Decimal logarithm of the maximum of the amplitude $A0_{max}$, corrected from attenuation, as a function of the decimal logarithm of the average momentum $|p|$ of the block before the impact. b) Decimal logarithm of the seismic energy E_s of the seismic signal generated at the impact as a function of the decimal logarithm of the kinetic energy before the impact E_k. c) Decimal logarithm of the seismic energy E_s as a function of the decimal logarithm of the masses of the blocks. d) Decimal logarithm of the seismic energy E_s of the seismic signal generated at the impact as a function of the decimal logarithm of the potential energy lost E_p. e) Decimal logarithm of the seismic energy E_s as a function of the decimal logarithm of the parameter $mV_z^{0.5}$. f) Decimal logarithm of the seismic energy E_s as a function of the decimal logarithm of the parameter $mV_z^{13/5}$. Errors bars resulting from the computation of the momentum, the kinetic energy and the amplitude at the source are indicated by black lines.

four cases regression lines of the data set to investigate possible correlation between the selected quantities. As all the point distribution appears to be following a linear trend (Figure 4), we computed the best regression line following equation:

$$Y = \alpha X + \beta, \tag{5}$$

Earth Surf. Dynam. Discuss., doi:10.5194/esurf-2016-64, 2017
Manuscript under review for journal Earth Surf. Dynam.
Published: 10 January 2017

with the parameter α and β of the regression line given in Table 2 for each case, in the logarithmic and linear scales. The best correlation is found between the maximum amplitude $A0_{max}$ and the momentum $|p|$, and the seismic energy E_s and the kinetic energy E_k, with R^2 values of 0.64. There is no significant correlation between the mass m and the seismic energy E_s as suggested by the low R^2 values of 0.31 and 0.39 of the regression lines. Overall the R^2 values do not exceed 0.64, which is caused by the high variability of the data. This high variability comes from the high uncertainties on the computation of the seismic attenuation parameters which in return impact the computed values of $A0_{max}$ and E_s, as shown by the large error bars on Figure 4. We also investigated other correlations between dynamic parameters and seismic signal features, with the vertical momentum or the vertical kinetic energy for example, but we were unable to improve on the correlations found with the modulus of the dynamic quantities.

The analysis based on the Hertz's theory of impact conducted by Farin et al. (2015) yielded the parameter $mV_z^{13/5}$, with m the mass of the block and V_z the vertical velocity before impact, that should in theory scale with the seismic energy E_s generated at each impact. However, when investigating this relationship for real single-block rockfalls, they did not found a significant correlation with this parameter. The best correlation they found was with the parameter $mV_z^{0.5}$. We investigated the two cases with our data set. We found that the parameter derived from Hertz's theory of impact yields a better correlation than the optimal parameter found in Farin et al. (2015), with R^2 values of 0.57–0.63 and 0.47–0.49 respectively (Figure 5e, f, and Table 2).

4.2 Retrieving block properties and dynamics from the seismic signal

We have shown that correlations exist between some dynamics quantities and features of the seismic signal generated at each impact. In this section we investigate if these relationships can provide accurate estimates of the mass and the velocity of the blocks, directly from the features of the seismic signal generated by impacts.

By combining Eq. (5) for the maximum amplitude and the momentum, and for the seismic energy and the kinetic energy, with the coefficients α and β computed in the linear scale, we can express the mass as a function of $A0_{max}$ and E_s as:

$$m_i = \frac{5.9 \times 10^{11}(A0_{max} - 2.50 \times 10^{-7})^2}{(Es + 0.01)}. \quad (6)$$

Using Eq. (6), we computed m_i for each impact of each block for which we were able to compute $A0_{max}$ and E_s, and compared the average estimates of m_i to the measured mass m_r of each block (Table 1). Overall, the inferred masses are close to the real masses of the block. However, the uncertainty on the inferred values is high, especially for block for which we have a few number of exploitable impacts and therefore few estimates of $A0_{max}$ and E_s. This may also come from the uncertainties related to the computation of the seismic quantities.

We can also estimate the velocity of the block before each impact using Eq. 5 with the correlation parameters found between the maximum amplitude $A0_{max}$ and the maximum momentum p, or between the seismic energy E_s and the kinetic energy E_k, and with the masses inferred with Eq. 6. We choose to use the relationship between the amplitude and the momentum because the uncertainties on the determination of the amplitude at the source are lower than the one on the seismic energy.

Earth Surf. Dynam. Discuss., doi:10.5194/esurf-2016-64, 2017
Manuscript under review for journal Earth Surf. Dynam.
Published: 10 January 2017

Figure 5a shows the distribution of the absolute difference between the velocities inferred V_i and the velocities V_r derived from the trajectory reconstruction. The values of the difference are comprised between 0.1 and 13.7 $\mathrm{m\,s^{-1}}$, with a median value of 2.4 $\mathrm{m\,s^{-1}}$. We also computed the ratio of the velocities difference over the velocities derived from the trajectory reconstruction (Figure 5b). The majority of the values of the ratio falls below 0.5 (i.e. the difference is less than 50% of the value of the velocity derived from the trajectory reconstruction), and the median ratio is 0.2 (i.e. 20% of the value of the velocity derived from the trajectory reconstruction).

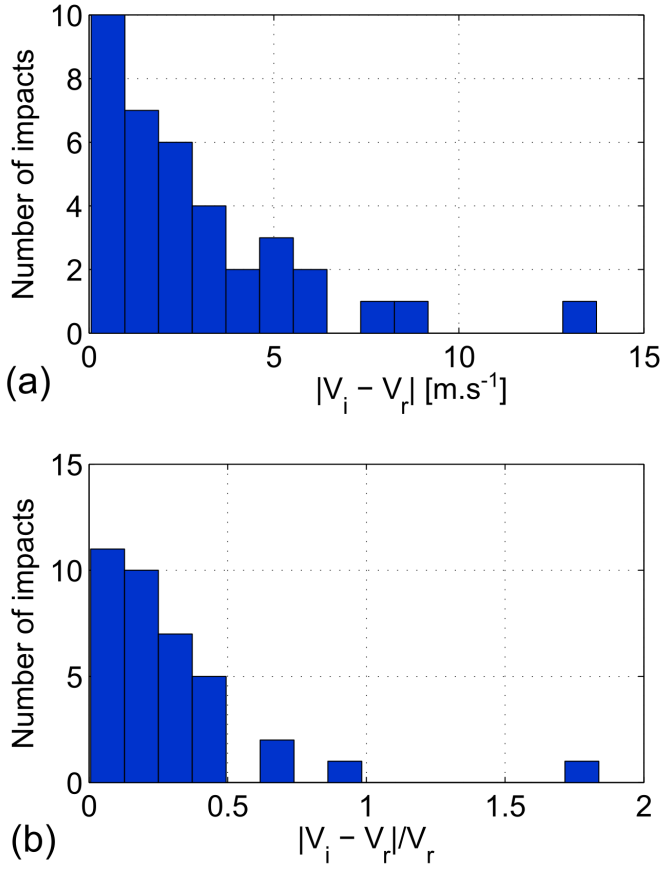

Figure 5. a) Histrogram showing the distribution of the difference between the velocity before impact V_i inferred using Eq. 5 and Eq. 3 and the velocity V_r estimated thanks to the video cameras; b) Same as a) but normalized by the value of the velocity V_r estimated via the video cameras.

Earth Surf. Dynam. Discuss., doi:10.5194/esurf-2016-64, 2017
Manuscript under review for journal Earth Surf. Dynam.
Published: 10 January 2017

5 Discussion and conclusion

The Rioux-Bourdoux experiment of controlled single-block rockfalls yields important results for understanding the links between the dynamics of rockfalls and the seismic signal associated. Our results suggest that linear scaling exist between the seismic signal features and the dynamic quantities of single-block rockfalls. We observed that the amplitude of the seismic signal generated at each impact and the momentum (product of the mass and the velocity) of the blocks are correlated. Our results also suggest that the energy of the seismic radiation released at each impact scales linearly with the potential energy lost and the kinetic energy. Despite large uncertainties, mainly caused by the simple seismic attenuation model used, the scaling laws found permit to infer realistic values of the masses and the velocities before impact of the blocks from the amplitude and the energy of the seismic signal generated.

We found that the relationship derived from the Hertz's theory of impact proposed by Farin et al. (2015) that links the seismic energy of the signal generated to the parameter $mV_z^{13/5}$ is verified with our data. This scaling was not confirmed for controlled single-block rockfalls in their study. They assume this was caused by the changing properties of the soil along the path and the low sampling frequency of the seismometer used that prevented to measure the totality of the seismic energy released at each impact. In our study the instruments we deployed permitted to record most of the energy generated at impacts. This underlines the importance of choosing adequate seismometers, capable of recording the whole seismic energy generated at the impacts, for future studies.

The scaling between the seismic energy and the parameter $mV_z^{13/5}$ did not yield a better quantitative correlation than the one observed between the seismic energy and the kinetic energy, or between the amplitude at the source and the momentum of the block before impact (best R^2 of 0.63, 0.64 and 0.64 respectively). This confirms the combined role of the mass and the velocity before impacts of the block in the generation of seismic waves, but does not allow us to identify a unique dynamic parameter that would control the seismic signal features. Further analytic and theoretical developments are needed to understand the physical processes that explain these correlations, and ultimately what are the physical parameters that control the characteristics of the seismic signal generated.

These relationships open the possibility to estimate directly the mass and the dynamic parameters of single-block rockfalls from the generated seismic signal. However, we identified several limitations that have to be addressed before considering an operational application of seismology to quantify rockfall properties. First, our results show that better attenuation models are needed to reduce the uncertainties on the computation of the seismic signal features. Second, the coefficients of the scaling laws we found between the different quantities may be controlled by the geological context. More similar studies performed in other contexts are needed to assess their potential impact on these relationships. Third, the range of the mass of the blocks used in our experiment spans only one order of magnitude. The behavior of the relationships we found has to be investigated for a larger range of volumes.

Finally, our results give a new insight on the processes that generate high-frequency seismic signals associated with rockfalls, landslides, rock-avalanches, and granular flows in general. We show that the maximum amplitude of the seismic signal generated by the impact of a single particle is proportional to its momentum. In a granular flow, a very large quantity of parti-

Earth Surf. Dynam. Discuss., doi:10.5194/esurf-2016-64, 2017
Manuscript under review for journal Earth Surf. Dynam.
Published: 10 January 2017

cles interacts with themselves and with the substrate at a given time. The source of the seismic signal generated at this given time might therefore be the sum of the impulses imparted by the particles to the ground. The magnitude of these impulses may be controlled by the momentum of the particles within the flow according to the scaling law we found. The issue is now to understand what controls the momentum of the particles within the flow. This should be more thoroughly investigated, using numerical granular flow models for example, and is probably the key to model the high-frequency seismic signal associated with gravitational instabilities in the future.

6 Code and Data availability

The codes and the data used in this study are accessible upon request by contacting C. Hibert (hibert@unistra.fr).

Author contributions. C. Hibert, J.-P. Malet, F. Bourrier and F. Provost participated in the acquisition and the processing of the seismic and kinematic data. F. Berger, P. Tardif and E. Mermin helped to design and perform the Rioux Bourdoux experiment, and for the acquisition of the video and the reconstruction of the trajectories of the blocks. P. Bornemann performed the Lidar survey and the processing of the data that allow to reconstruct the DEM of the gully into which blocks have been launched.

Competing interests. The authors declare that they have no conflict of interest.

Acknowledgements. We are very grateful toward Anne Mangeney for helpful discussions and insightful suggestions. This work was carried with the support of the French National Research Agency (ANR) through the projects HYDROSLIDE 'Hydrogeophysical Monitoring of Clayey Landslides' and SAMCO 'Adaptation de la Société aux Risques Gravitaires en Montagne dans un Contexte de Changement Global' and of the Open Partial Agreement Major Hazards of Council of Europe through the project 'Development of cost-effective ground-based and remote monitoring systems for detecting landslide initiation'. The seismometers used in this experiment belong to the French national pool of portable seismicinstruments SISMOB-RESIF.

Earth Surf. Dynam. Discuss., doi:10.5194/esurf-2016-64, 2017
Manuscript under review for journal Earth Surf. Dynam.
Published: 10 January 2017

References

Aki, K. and Chouet, B.: Origin of coda waves: source, attenuation, and scattering effects, Journal of geophysical research, 80, 3322–3342, 1975.

Allstadt, K.: Extracting source characteristics and dynamics of the August 2010 Mount Meager landslide from broadband seismograms, Journal of Geophysical Research, 118, 1472–1490, doi:10.1002/jgrf.20110, 2013.

Burtin, A., Hovius, N., Milodowski, D. T., Chen, Y.-G., Wu, Y.-M., Lin, C.-W., Chen, H., Emberson, R., and Leu, P.-L.: Continuous catchment-scale monitoring of geomorphic processes with a 2-D seismological array, Journal of Geophysical Research: Earth Surface, 118, 1956–1974, 2013.

Chen, C.-H., Chao, W.-A., Wu, Y.-M., Zhao, L., Chen, Y.-G., Ho, W.-Y., Lin, T.-L., Kuo, K.-H., and Chang, J.-M.: A seismological study of landquakes using a real-time broad-band seismic network, Geophysical Journal International, 194, 885–898, 2013.

Clouard, V., Athanase, J.-E., and Aubaud, C.: Physical characteristics and triggering mechanisms of the 2009–2010 landslide crisis at Montagne Pelée volcano, Martinique: implication for erosional processes and debris-flow hazards, Bulletin de la Société Géologique de France, 184, 155–164, 2013.

Crampin, S.: Higher modes of seismic surface waves: Second Rayleigh mode energy, Journal of Geophysical Research, 70, 5135–5143, 1965.

Dammeier, F., Moore, J. R., Haslinger, F., and Loew, S.: Characterization of alpine rockslides using statistical analysis of seismic signals, Journal of Geophysical Research, 116, F04 024, doi:10.1029/2011JF002037, 2011.

Dammeier, F., Moore, J. R., Hammer, C., Haslinger, F., and Loew, S.: Automatic detection of alpine rockslides in continuous seismic data using Hidden Markov Models, Journal of Geophysical Research: Earth Surface, 121, 351–371, 2016.

Deparis, J., Jongmans, D., Cotton, F., Baillet, L., Thouvenot, F., and Hantz, D.: Analysis of rock-fall and rock-fall avalanche seismograms in the French Alps, Bulletin of the Seismological Society of America, 98, 1781–1796, doi:10.1785/0120070082, 2008.

Ekström, G. and Stark, C. P.: Simple scaling of catastrophic landslide dynamics, Science, 339, 1416–1419, doi:10.1126/science.1232887, 2013.

Farin, M., Mangeney, A., Toussaint, R., Rosny, J. d., Shapiro, N., Dewez, T., Hibert, C., Mathon, C., Sedan, O., and Berger, F.: Characterization of rockfalls from seismic signal: Insights from laboratory experiments, Journal of Geophysical Research: Solid Earth, 120, 7102–7137, doi:10.1002/2015JB012331, 2015JB012331, 2015.

Favreau, P., Mangeney, A., Lucas, A., Crosta, G., and Bouchut, F.: Numerical modeling of landquakes, Geophysical Research Letters, 37, L15 305, doi:10.1029/2010GL043512, 2010.

Gance, J., Grandjean, G., Samyn, K., and Malet, J.-P.: Quasi-Newton inversion of seismic first arrivals using source finite bandwidth assumption: Application to subsurface characterization of landslides, Journal of Applied Geophysics, 87, 94–106, 2012.

Helmstetter, A. and Garambois, S.: Seismic monitoring of Séchilienne rockslide (French Alps): Analysis of seismic signals and their correlation with rainfalls, Journal of Geophysical Research, 115, F03 016, doi:10.1029/2009JF001532, 2010.

Hertz, H.: Über die Berührung fester elastischer Körper., Journal für die reine und angewandte Mathematik, 92, 156–171, 1882.

Hibert, C., Mangeney, A., Grandjean, G., and Shapiro, N. M.: Slope instabilities in Dolomieu crater, Réunion Island: From seismic signals to rockfall characteristics, Journal of Geophysical Research, 116, F04 032, doi:10.1029/2011JF002038, 2011.

Hibert, C., Grandjean, G., Bitri, A., Travelletti, J., and Malet, J.-P.: Characterizing landslides through geophysical data fusion: Example of the La Valette landslide (France), Engineering Geology, 128, 23–29, 2012.

Hibert, C., Ekström, G., and Stark, C. P.: Dynamics of the Bingham Canyon Mine landslides from seismic signal analysis, Geophysical Research Letters, 41, 4535–4541, doi:10.1002/2014GL060592, 2014a.

Hibert, C., Mangeney, A., Grandjean, G., Baillard, C., Rivet, D., Shapiro, N. M., Satriano, C., Maggi, A., Boissier, P., Ferrazzini, V., and Crawford, W.: Automated identification, location, and volume estimation of rockfalls at Piton de la Fournaise volcano, Journal of Geophysical Research: Earth Surface, 119, 1082–1105, doi:10.1002/2013JF002970, http://dx.doi.org/10.1002/2013JF002970, 2014b.

Hibert, C., Stark, C. P., and Ekström, G.: Seismology of the Oso-Steelhead landslide, Nat. Hazards Earth Syst. Sci. Discuss., pp. 7309–7327, 2014c.

Hibert, C., Ekström, G., and Stark, C. P.: The relationship between bulk-mass momentum and short-period seismic radiation in catastrophic landslides, Submited to Journal of Geophysical Research: Earth Surface, 2017.

Levy, C., Mangeney, A., Bonilla, F., Hibert, C., Calder, E. S., and Smith, P. J.: Friction weakening in granular flows deduced from seismic records at the Soufrière Hills Volcano, Montserrat, Journal of Geophysical Research: Solid Earth, 120, 7536–7557, 2015.

Maquaire, O., Malet, J.-P., Remaıtre, A., Locat, J., Klotz, S., and Guillon, J.: Instability conditions of marly hillslopes: towards landsliding or gullying? The case of the Barcelonnette Basin, South East France, Engineering Geology, 70, 109–130, 2003.

Moretti, L., Mangeney, A., Capdeville, Y., Stutzmann, E., Huggel, C., Schneider, D., and Bouchut, F.: Numerical modeling of the Mount Steller landslide flow history and of the generated long period seismic waves, Geophysical Research Letters, 39, L16 402, doi:10.1029/2012GL052511, 2012.

Norris, R. D.: Seismicity of rockfalls and avalanches at three Cascade Range volcanoes: Implications for seismic detection of hazardous mass movements, Bulletin of the Seismological Society of America, 84, 1925–1939, 1994.

Schneider, D., Bartelt, P., Caplan-Auerbach, J., Christen, M., Huggel, C., and McArdell, B. W.: Insights into rock-ice avalanche dynamics by combined analysis of seismic recordings and a numerical avalanche model, Journal of Geophysical Research, 115, F04 026, doi:10.1029/2010JF001734, 2010.

Tripolitsiotis, A., Daskalakis, A., Mertikas, S., Hristopulos, D., Agioutantis, Z., and Partsinevelos, P.: Detection of small-scale rockfall incidents using their seismic signature, in: Third International Conference on Remote Sensing and Geoinformation of the Environment, pp. 953 519–953 519, International Society for Optics and Photonics, 2015.

Yamada, M., Matsushi, Y., Chigira, M., and Mori, J.: Seismic recordings of landslides caused by Typhoon Talas (2011), Japan, Geophysical Research Letters, 39, L13 301, doi:10.1029/2012GL052174, 2012.

Yamada, M., Kumagai, H., Matsushi, Y., and Matsuzawa, T.: Dynamic landslide processes revealed by broadband seismic records, Geophysical Research Letters, 40, 2998–3002, doi:10.1002/grl.50437, 2013.

Zimmer, V. L. and Sitar, N.: Detection and location of rock falls using seismic and infrasound sensors, Engineering Geology, 193, 49–60, 2015.

Earth Surf. Dynam. Discuss., doi:10.5194/esurf-2016-64, 2017
Manuscript under review for journal Earth Surf. Dynam.
Published: 10 January 2017

Earth Surface Dynamics Discussions
Open Access
EGU

Block #	m_r [kg]	m_i [kg]	std.	Nbr. impacts
9	281	198	56	5
1	318	334	71	6
4	209	208	115	7
35	82	84	68	3
33	256	97	-	1
22	154	171	146	3
20	198	211	39	6
17	136	181	118	4
13	140	270	162	2

Table 1. Comparison between the real mass m_r of the blocks and the average inferred masses m_i computed with Eq. 6.

	logarithm			linear		
Parameters (X, Y)	α	β	R^2	α	β	R^2
$A0_{max} = \alpha\, p + \beta$	0.84	-8.12	0.58	$2.26\,10^{-9}$	$2.50\,10^{-7}$	0.64
$E_s = \alpha\, E_p + \beta$	-1.17	-6.05	0.54	$-5.04\,10^{-6}$	-0.01	0.61
$E_s = \alpha\, E_k + \beta$	1.38	-7.34	0.60	$3.09\,10^{-6}$	-0.01	0.64
$E_s = \alpha\, m + \beta$	1.9	-6.23	0.39	$2.85\,10^{-4}$	-0.03	0.31
$E_s = \alpha\, m V_z^{13/5} + \beta$	1.43	-8.60	0.57	$5.85\,10^{-7}$	-0.01	0.63
$E_s = \alpha\, m V_z^{0.5} + \beta$	2.02	-7.42	0.49	$1.07\,10^{-4}$	-0.04	0.47

Table 2. Coefficients of the regression lines